Journal of Computational Acoustics, Vol. 18, No. 3 (2010) 227–243

DOI: 10.1142/S0218396X10004140

INTERNATIONAL ASSOCIATION
FOR MATHEMATICS AND
COMPUTERS IN SIMULATION

VOLUME CLUTTER ELIMINATION, ROUGH INTERFACE REVERBERATION SUPPRESSION, AND TARGET RESONANCE CONVERGENCE IN HETEROGENEOUS MEDIA USING AN ITERATIVE TIME REVERSAL MIRROR

YINGZI YING* and LI MA

Institute of Acoustics, Chinese Academy of Sciences
21 Beisihuanxi Road, Beijing 100190, China
**yingyz05@mails.gucas.ac.cn*

Received 29 December 2009
Revised 21 June 2010

The presence of the clutter of volume scattering and the echo return from rough interface hinders the detection of target in heterogeneous media. This work investigates the application of an iterative time reversal mirror to mitigate the difficulties. Numerical simulations based on pseudospectral finite-difference time-domain method are performed in one and two layered media. A wideband probe pulse is launched to initiate the process, and the time-reversed echo received at the same position is retransmitted as the renewed input signal for next iteration, and repeat the procedures iteratively. The results illustrate as the number of iteration increases, small volume clutter is eliminated, interface reverberation is suppressed relatively, and the echoes will converge to a time-harmonic waveform that corresponds to an object's dominant resonance mode. The detection of target is achieved by extracting this important acoustic signature.

Keywords: Multiple scattering; resonance convergence; iterative time reversal.

1. Introduction

Wave propagation and time reversal in heterogeneous media, where the multipath and multiple scattering are observable, will increase the spatial focusing and time compression, thus to enhance the effective array aperture,[1,2] and the retrofocused field will exhibit self-averaging property and is statistical stable.[3] Time reversal has been investigated in focusing through chaotic cavities,[4] acoustic imaging in random media,[3] adaptive interference cancellation in cluttered electromagnetic domain,[5] etc.

The resonance spectrogram of object could be recognized as its fingerprint, which is the intrinsic characteristics that depends on the geometry and material composition. The resonance scattering from submerged elastic objects of typical shapes such as spheres and cylinders are analyzed,[6] and hollow spheres with either water or air in interior,[7] as well as anisotropic conditions.[8]

The iterative time reversal[9,10] is initially demonstrated to focus energy on the most reflective scatterer efficiently. The analysis[11] shows the iterative process involving a time

reversal mirror could automatically obtain the optimal incident field to achieve the maximum distinguishability between the target and background in acoustic imaging. The tank experiments[12] are performed with a spherical shell, a small stone, and a complex steel object as targets, and the results indicate the single channel iterative time reversal would provide significant echo enhancement, thus to improve the single-to-noise ratio. Numerical studies[13] demonstrate the iterative time reversal process will gradually lead echoes to converge to a narrowband signal, in which the analysis is mainly based on the case of a rigid sphere in homogeneous half-space.

In this work, the iterative time reversal will take effect as an adaptive matched filter for the spectral response of the scattering of the most reflective scatterer in heterogeneous media. Since the wave equation in nondispersive and motionless field supports time reversal invariance and spatial reciprocity, the iterative process will gradually eliminate small scattering such as volume clutter and interface reverberation, and the echoes will converge to a resonance mode of the most reflective scatterer eventually. The theoretical analysis will take the multiple scattering effects into consideration and the numerical simulations are performed in one and two layered heterogeneous media. Figure 1(a) depicts a typical realization of the deployment, in which several spherical targets are partially or fully buried in the bottom, and a time reversal mirror is deployed horizontally in the water column, whose elements are a transmitter and receiver couples. Figure 1(b) illustrates the process of iterative time reversal, that initially illuminate the target with a broadband interrogation pulse, measure and filter the echo, reverse the data stream in time domain and send it back, and repeat the procedures iteratively.

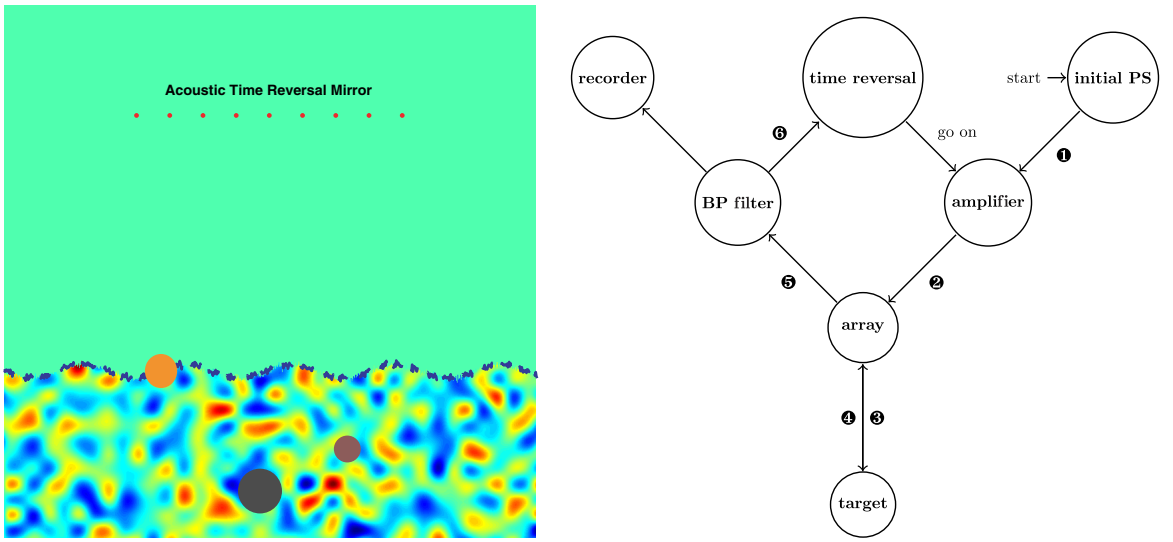

(a) (b)

Fig. 1. (a) Deployment illustration; (b) flow chart of the iterative time reversal in target detection.

2. Theory

2.1. *Array inter-element response and time-reversal operator in heterogeneous media*

We first consider the Green's function G that satisfies the nonhomogeneous wave equation,

$$\left(\nabla\cdot\left(\frac{1}{\rho(\mathbf{r})}\nabla\right)-\frac{1}{\rho(\mathbf{r})c_0^2}n^2(\mathbf{r})\partial_{tt}\right)G(\mathbf{r},t;\mathbf{r}_0,t_0)=-\delta(\mathbf{r}-\mathbf{r}_0)\delta(t-t_0), \tag{1}$$

in which c_0 is the reference sound velocity, $n(\mathbf{r})=c_0/c(\mathbf{r})$ is the refraction index of the heterogeneous media with the random sound velocity $c(\mathbf{r})$, and δ is the Dirac delta function.

Assume an array has M same transceivers, whose transmission and reception acousto-electric transformation coefficients are a_e and a_r, respectively, and take L targets into consideration. First, the initial probe signals are emanated by the array, propagate forward, scattered by the targets, back propagate and at last received by the array. The round trip of the signals could be viewed as going through a linear time invariant system expressed with a transfer matrix,

$$\mathbf{h}=\mathbf{a}_\mathrm{r}\mathbf{g}^\mathrm{t}\mathbf{c}\mathbf{g}\mathbf{a}_\mathrm{e}. \tag{2}$$

Here, $\mathbf{a}_\mathrm{e}=\mathrm{diag}(a_\mathrm{e})$ and $\mathbf{a}_\mathrm{r}=\mathrm{diag}(a_\mathrm{r})$ are M-dimension diagonal matrices. $\mathbf{g}\in\mathbb{C}^{L\times M}$ is the forward diffraction matrix and its element inputs $g(\mathbf{r}_{\mathrm{s}_l},\omega;\mathbf{r}_{\mathrm{t}_m})=\mathcal{F}_t(G(\mathbf{r}_{\mathrm{s}_l},t;\mathbf{r}_{\mathrm{t}_m}))(\omega)$, are the harmonic Green's functions from mth transceiver to lth scatterer, and $\mathcal{F}\colon L^2(\mathbb{R})\to L^2(\mathbb{R})$ denotes the Fourier transform operator, i.e., $\mathcal{F}_t(\cdot(t))(\omega)=\int_{\mathbb{R}}\cdot(t)\mathrm{e}^{-\mathrm{i}\omega t}\mathrm{d}t$. Then the transposed form $\mathbf{g}^\mathrm{t}$ is the backward diffraction matrix, and superscript t is the matrix transpose operator. According to the reciprocity principle, reflectivity coefficient matrix $\mathbf{c}\in\mathbb{C}^{L\times L}$ is symmetric, and its diagonal inputs are reflectivity coefficients and off-diagonals are multiple scattering components. The definition of the reflectivity coefficient matrix is given in A, and the multiple scattering effects are taken into consideration because Green's functions to the stochastic wave equation are random in heterogeneous media.[3] Obviously, $\mathbf{h}$ is a symmetric matrix.

The so called time reversal operator $\mathbf{h}^*\mathbf{h}$, is a positive defined Hermitian matrix, and we arrange its real eigenvalues in a descending order, $\lambda_1>\cdots>\lambda_L>\lambda_{L+1}\approx\cdots\approx\lambda_M\approx 0$. The eigenvalues are not fully degenerated as adequate scatterers exist in heterogeneous media. Time reversal conducted in the time domain is equivalent to a phase conjugation in the Fourier domain, and we use superscript $*$ to denote the complex conjugate operator.

2.2. *Small scattering elimination and iterative convergence*

Assume the initial interrogation vector $\mathbf{e}_0=(e_{0m})$ is loaded on the array for the initial illumination, then the measured and time reversed echo vector of the first iteration is $\mathbf{h}^*\mathbf{e}_0^*$, and of the second iteration is $\mathbf{h}^*\mathbf{h}\mathbf{e}_0$, and so on. As Hermitian matrix is diagonalizable,

we can decompose the $2n$th iterative time reversal matrix $(\mathbf{h}^*\mathbf{h})^n$ into the eigenvalues and eigenvectors:

$$(\mathbf{h}^*\mathbf{h})^n = (\mathbf{u}\boldsymbol{\lambda}\mathbf{u}^{-1})^n = \mathbf{u}\boldsymbol{\lambda}^n\mathbf{u}^{-1}, \tag{3}$$

where $\boldsymbol{\lambda} = \mathrm{diag}(\lambda_m)$ is the diagonal matrix of the eigenvalues, and $\mathbf{u} = (\mathbf{u}_m)$ is the corresponding eigenvector matrix and $\mathbf{u}_m$ satisfy the eigenvalue equations of the time reversal matrix,

$$\mathbf{h}^*\mathbf{h}\mathbf{u}_m = \lambda_m\mathbf{u}_m, \quad m \le M. \tag{4}$$

Since the eigenvectors of Hermitian matrix are orthogonal, and make them unit norm, that is $(\mathbf{u}_m, \mathbf{u}_{m'}) = \delta_{mm'}$, where the operator $(\cdot,\cdot)$ is the inner product in the complex vector space, and $\delta_{mm'}$ is the Kronecker delta. We can get $\mathbf{u}^\dagger\mathbf{u} = \mathbf{i}$, and superscript $\dagger$ denotes the conjugate transpose and $\mathbf{i}$ is the identity matrix. This means that the eigenvector matrix $\mathbf{u}$ is unitary, that is $\mathbf{u}^{-1} = \mathbf{u}^\dagger$, then the $2n$th iterative time reversal matrix might be expressed as

$$(\mathbf{h}^*\mathbf{h})^n = \mathbf{u}\lambda_1^n \begin{pmatrix} 1 & & & & & & \\ & (\lambda_2/\lambda_1)^n & & & & & \\ & & \ddots & & & & \\ & & & (\lambda_L/\lambda_1)^n & & & \\ & & & & \ddots & & \\ & & & & & (\lambda_M/\lambda_1)^n \end{pmatrix} \mathbf{u}^\dagger. \tag{5}$$

For a large iteration number, we can assume $(\lambda_m/\lambda_1)^n \approx 0$, for all $m \ge 2$, then the renewed array input vector after $2n$th iteration will approximates to,

$$\mathbf{e}_{2n} = (\mathbf{h}^*\mathbf{h})^n\mathbf{e}_0 \approx \lambda_1^n\mathbf{u}_1\mathbf{u}_1^\dagger\mathbf{e}_0. \tag{6}$$

And the initial interrogation vector $\mathbf{e}_0(\omega)$ could be projected onto the complete orthonormal basis set $\{\mathbf{u}_m\}_{1\le m\le M}$, that is $\mathbf{e}_0 = \sum_{m=1}^M a_m\mathbf{u}_m$, and the mth coordinate is $a_m = (\mathbf{u}_m, \mathbf{e}_0)$.

According to the property of exponential function, the normalized form of the modulus of the echo vector will converge to

$$|\bar{\mathbf{e}}_{2n}(\omega)| \to \mathbf{1}_{\{\omega:\boldsymbol{\omega}=\boldsymbol{\omega_0}\}}(\omega) \quad \text{as } n \to \infty, \tag{7}$$

where the indicator function of the set A is

$$\mathbf{1}_A(\omega) = \begin{cases} 1 & \text{if } \omega \in A, \\ 0 & \text{if } \omega \in A^c, \end{cases} \tag{8}$$

and $\boldsymbol{\omega}_0 = (\omega_0)$ is the converged frequency vector, in which

$$\omega_0 := \arg\max_{\omega\in[\omega_1,\omega_2]} |\lambda_1(\omega)|, \tag{9}$$

and the frequency interval $[\omega_1, \omega_2]$ is selected by a bandpass filter.

Equation (7) denotes the iterative time reversal process will lead the echoes received by the elements of the array to converge to the same narrowband signal, whose frequency corresponds to a maximum of the modulus of the largest eigenvalue of the time reversal matrix according to Eq. (9).

2.3. *Eigenvalue determination*

The lth row of the diffraction matrix $\mathbf{g}_{l*}$ is the transfer vector from the array to the lth scatterer, and we denote the conjugated and normalized version $\bar{\mathbf{g}}_{l*}^{*} = \mathbf{g}_{l*}^{*}/\|\mathbf{g}_{l*}\|$ in a vector form, that is divided by its Euclidean norm. When scatterers are well separated from each other, the transfer vectors corresponding to different scatterers are orthogonal due to the spacial decay of Green's functions and destructive interference,[3] that is $\mathbf{g}_{l*} \perp \mathbf{g}_{l'*}$ for all $l \neq l'$, or quasi-orthogonal in more real situation. So the elements of the orthonormal bases set $\mathcal{B} = \{\bar{\mathbf{g}}_{l*}^{*}\}_{1\leq l\leq L}$ that spans a subspace $S = \text{span}\{\mathcal{B}\} \subseteq \mathbb{C}^M$ can be deployed as the eigenvectors of the time reversal matrix $\mathbf{h}^*\mathbf{h}$, while the eigenvectors $\bar{\mathbf{g}}_{l*}^{*}$ are orthogonal to this linear hull for $L < l \leq M$.

We can get the associated eigenvalues according to the properties of Hermitian matrix and orthonormal bases,

$$\lambda_l = \frac{(\mathbf{h}^*\mathbf{h}\bar{\mathbf{g}}_{l*}^{*}, \bar{\mathbf{g}}_{l*}^{*})}{(\bar{\mathbf{g}}_{l*}^{*}, \bar{\mathbf{g}}_{l*}^{*})} = \frac{(\bar{\mathbf{g}}_{l*}^{*}, \mathbf{h}^*\mathbf{h}\bar{\mathbf{g}}_{l*}^{*})}{(\bar{\mathbf{g}}_{l*}^{*}, \bar{\mathbf{g}}_{l*}^{*})} = \bar{\mathbf{g}}_{l*}^{\mathrm{t}}\mathbf{h}^*\mathbf{h}\bar{\mathbf{g}}_{l*}^{*}, \quad l \leq L, \tag{10}$$

and substitute Eq. (2) into Eq. (10), we can get the expressions of eigenvalues that will be derived in B,

$$\lambda_l = |a_{\mathrm{e}}a_{\mathrm{r}}|^2\|\mathbf{g}_{l*}\|^2 \sum_{l'=1}^{L} \|\mathbf{g}_{l'*}\|^2 |c_{ll'}|^2, \quad l \leq L. \tag{11}$$

If we can ignore weak multiple scattering components, i.e., $c_{ll'} \approx 0$ for all $l \neq l'$, then the expressions are simplified as

$$\lambda_l \approx |a_{\mathrm{e}}a_{\mathrm{r}}|^2|c_{ll}|^2\|\mathbf{g}_{l*}\|^4, \quad l \leq L. \tag{12}$$

We can see the eigenvalue, which represents the strength of target, is mainly determined by its reflectivity coefficients and particular position in relation to the array.

If we select the frequency interval in the flat domain of the transceiver response, and ignore the propagation effect, which just plays a constant coefficient role in homogeneous media, the converged frequency will approximately correspond to a response peak of the scattering of the most reflective scatterer,

$$\omega_0 \approx \arg\max_{\omega\in[\omega_1,\omega_2]} |c_{11}(\omega)|. \tag{13}$$

In fact, the multiple scattering and propagation effects in heterogeneous media do alter the value of converged frequency.

3. Numerical Experiments

3.1. *Scattering properties of a liquid sphere*

We describe the scattering properties of object with resonance spectrogram, and take a liquid sphere D with radius a and immersed in water for example. Assume a plane harmonic wave $p^{\text{in}} = p_0 \exp(\mathrm{i}kr\cos\theta)$ is incident on the sphere, which is expanded by the superposition of individual normal modes

$$p^{\text{in}} = p_0 \sum_{m=0}^{\infty} (2m+1)\mathrm{i}^m \mathrm{j}_m(kr)\mathrm{P}_m(\cos\theta) \quad \text{in } \mathbb{R}^3\backslash D, \tag{14}$$

where k is the wave number in water, j_m is the mth-order spherical Bessel function of the first kind, and P_m is the Legendre polynomial. And the secondary scattered wave can also be expressed in a series form

$$p^{\text{sc}} = p_0 \sum_{m=0}^{\infty} (2m+1)\mathrm{i}^m a_m \mathrm{h}_m^{(1)}(kr)\mathrm{P}_m(\cos\theta) \quad \text{in } \mathbb{R}^3\backslash D, \tag{15}$$

where the spherical Hankel function has an asymptotic form for $kr \gg m$,

$$\mathrm{h}_m^{(1)}(kr) \sim \frac{1}{kr}\mathrm{i}^{-(m+1)}\exp(\mathrm{i}kr). \tag{16}$$

We express the transmitted pressure field in the sphere in a similar form

$$p^{\text{tr}} = p_0 \sum_{m=0}^{\infty} (2m+1)\mathrm{i}^m b_m \mathrm{j}_m(k_0 r)\mathrm{P}_m(\cos\theta) \quad \text{in } D, \tag{17}$$

here k_0 is the wave number in the liquid sphere and j_m is selected instead of h_m in order to avoid singular value at sphere center $r = 0$.

The coefficients a_m and b_m are determined by the continuities of the pressure and radial particle velocity on the boundary ∂D, i.e.,

$$\begin{cases} p^{\text{in}} + p^{\text{sc}} = p^{\text{tr}} & \text{on } \partial D, \\ v_r^{\text{in}} + v_r^{\text{sc}} = v_r^{\text{tr}} & \text{on } \partial D, \end{cases} \tag{18}$$

where the harmonic radial particle velocity is $v_r = \partial_r p/\mathrm{i}\rho\omega$. By comparing the coefficients of the Legendre polynomial $\mathrm{P}_m(\cos\theta)$ in Eq. (18), we can get

$$\begin{pmatrix} -\mathrm{h}_m^{(1)}(ka) & \mathrm{j}_m(k_0 a) \\ -\dfrac{\mathrm{h}_m^{(1)\prime}(ka)}{\rho} & \dfrac{\mathrm{j}_m'(k_0 a)}{\rho_0} \end{pmatrix} \begin{pmatrix} a_m \\ b_m \end{pmatrix} = \begin{pmatrix} \mathrm{j}_m(ka) \\ \dfrac{\mathrm{j}_m'(ka)}{\rho} \end{pmatrix}, \tag{19}$$

where ρ_0 and ρ are the density of the sphere and water, respectively. Then the coefficients a_m and b_m are obtained by solving Eq. (19), thus the pressure fields both in and outside the liquid sphere.

To identify the target information from the scattered field, the concept of the partial wave phase shift δ_m is introduced,[14]

$$2a_m + 1 \equiv \exp(2\mathrm{i}\delta_m), \tag{20}$$

as well as the partial form functions

$$f_m(\theta) := \frac{2}{ka}(2m+1)\exp(\mathrm{i}\delta_m)\sin\delta_m \mathrm{P}_m(\cos\theta), \tag{21}$$

and the form function is the superposition of the partial form functions

$$f(\theta) := \sum_{m=0}^{\infty} f_m(\theta). \tag{22}$$

Then we can get the asymptotic expression of the scattered pressure in far field by using Eq. (16),

$$p^{\mathrm{sc}} \sim p_0 \frac{a}{2r}\exp(\mathrm{i}kr) f(\theta). \tag{23}$$

The detection of target with iterative time reversal is investigated in a monostatic configuration, that is $\theta = \pi$, then the modulus of the reflectivity coefficient is proportional to the modulus of the form function,

$$|c(\omega)| \propto |f(\pi, \omega)|. \tag{24}$$

According to Eqs. (13) and (24), we know the converged frequency will correspond to a maximum of the modulus of the backscattering form function,

$$\omega_0 \approx \arg\max_{\omega\in[\omega_1,\omega_2]} |f(\pi,\omega)|, \tag{25}$$

that the echoes will converge to a resonance mode.

Figure 2(a) plots first four partial form functions of the liquid sphere submerged in water, whose parameters are given in Table 1, and Fig. 2(b) is the form function that is the superposition of the first 100 partial form functions. There are four resonance peaks for ka in the interval $[5, 10]$, which are about at 6.15, 7.35, 8.55, and 9.75.

3.2. *Acoustic pseudospectral finite-difference method*

We solve the following wave equation with pseudospectral finite-difference time-domain method,

$$\left(\nabla\cdot\left(\frac{1}{\rho(\mathbf{r})}\nabla\right) - \frac{1}{\rho(\mathbf{r})c^2(\mathbf{r})}\partial_{tt}\right)\phi(\mathbf{r},t) = -s(t)\mathbf{1}_{\{\mathbf{r}:\mathbf{r}=\mathbf{r}_{\mathrm{s}}\}}(\mathbf{r}) \quad \text{in } \mathbb{R}^2\times[0,T], \tag{26}$$

in which $\mathbf{r}_{\mathrm{s}}$ is the location of the isotropic point-source, and $s(t)$ is the source function. The spatial derivation is evaluated in the wave number domain:

$$\nabla(\cdot(\mathbf{r})) = \mathcal{F}_{\mathbf{k}}^{-1}(\mathrm{i}k\mathcal{F}_{\mathbf{r}}(\cdot(\mathbf{r}))(\mathbf{k}))(\mathbf{r}), \tag{27}$$

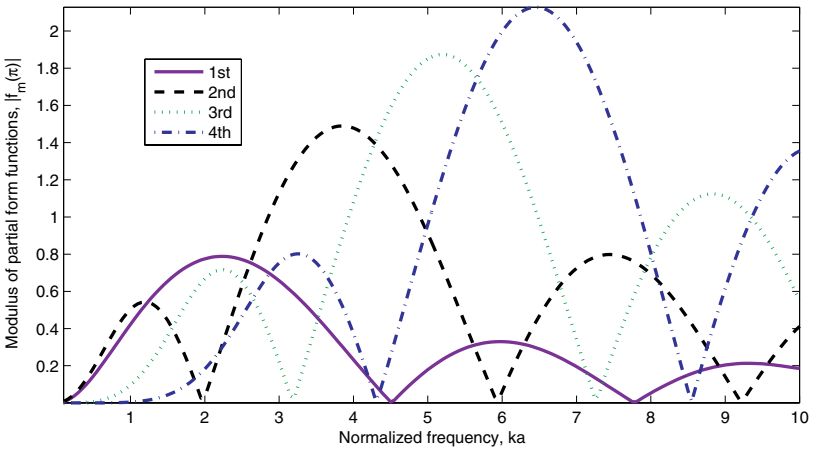

(a)

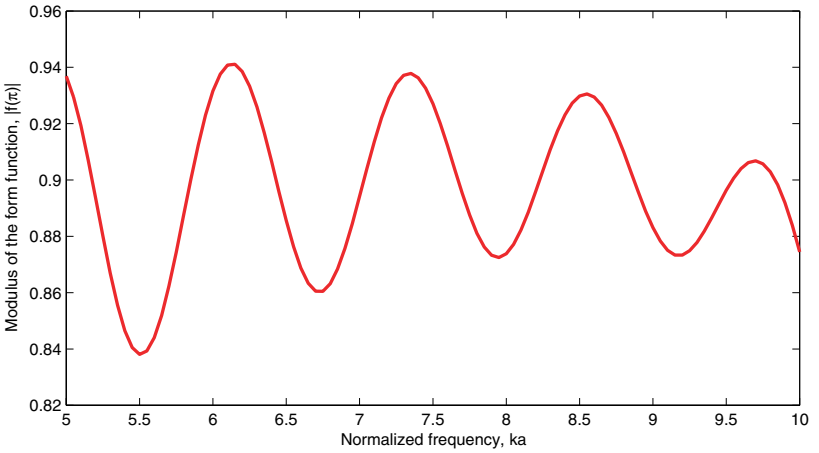

(b)

Fig. 2. (a) The modulus of the first four partial form functions of the liquid sphere $|f_m(\pi; ka)|$, plotted versus normalized frequency ka; (b) the modulus of the form function $|f(\pi; ka)|$.

Table 1. Parameters of the liquid sphere and water.

	Sound velocity (m/s)	Density (kg/m^3)
Sphere	4994	7900
Water	1495	1000

Note: Just is a steel ball ignored elasticity that set the Lamé shear modulus μ to zero.

here $\mathbf{k}$ is the propagation vector and $\mathcal{F}\colon L^2(\mathbb{R}^2) \to L^2(\mathbb{R}^2)$ is the two-dimensional unitary Fourier transform and $\mathcal{F}^{-1}$ is the reverse operator, i.e.,

$$\mathcal{F}_{\mathbf{r}}(\cdot(\mathbf{r}))(\mathbf{k}) = \frac{1}{2\pi}\int_{\mathbb{R}^2} \cdot(\mathbf{r})\mathrm{e}^{-\mathrm{i}\mathbf{k}\cdot\mathbf{r}}\mathrm{d}\mathbf{r}, \tag{28}$$

$$\mathcal{F}^{-1}_{\mathbf{k}}(\cdot(\mathbf{k}))(\mathbf{r}) = \frac{1}{2\pi}\int_{\mathbb{R}^2} \cdot(\mathbf{k})\mathrm{e}^{\mathrm{i}\mathbf{k}\cdot\mathbf{r}}\mathrm{d}\mathbf{k}. \tag{29}$$

The initial condition of the field is

$$\phi(\mathbf{r}, 0) = 0 \quad \text{in } \mathbb{R}^2. \tag{30}$$

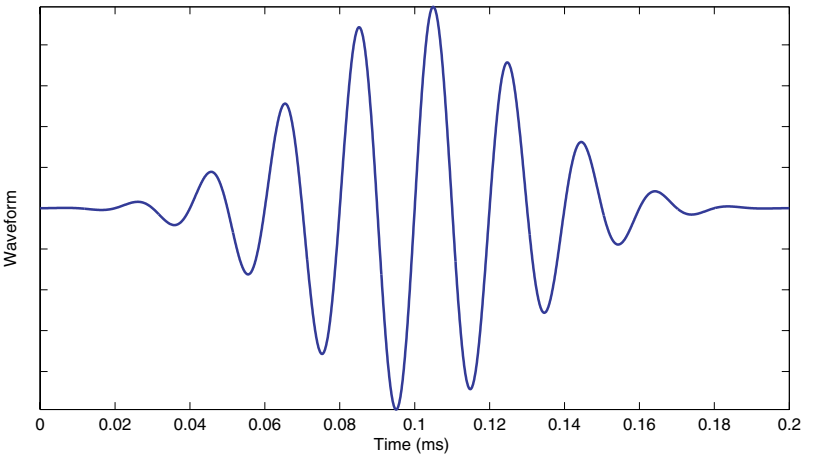

(a)

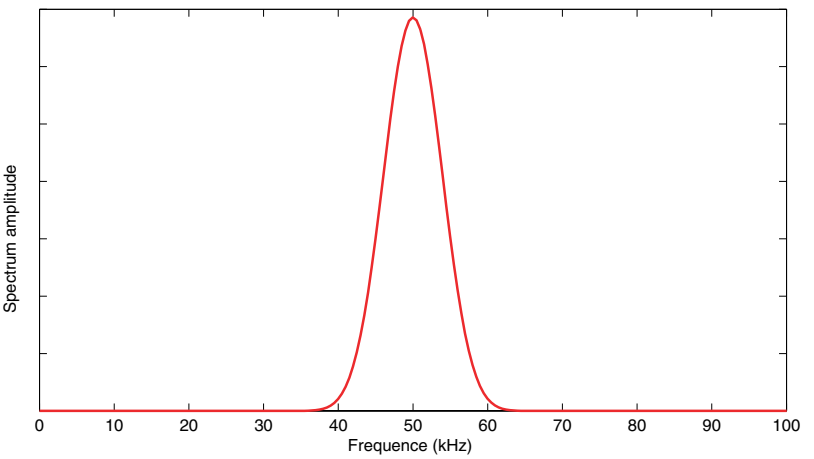

(b)

Fig. 3. (a) The initial interrogation pulse; (b) the respective frequency spectrum.

In order to avoid boundary reflection, a sponger layer is appended to the computational domain with a taper factor. Pseudospectral finite-difference method has higher accuracy for spatial derivation and less sampling rate is needed. The time derivation is calculated by normal implicit backward finite-difference approach.

3.3. *One layered media simulation*

In numerical experiments, a single channel array will be adopted, that is $\mathbf{a}_{\mathrm{e,r}} = \mathrm{diag}(a_{\mathrm{e,r}}, 0, \ldots, 0)$, and a liquid sphere with parameters given in Table 1 and 0.05 m radius is taken as the target. We select a Chebyshev window modulated on a 50 kHz sine carrier wave as the initial interrogation pulse, which is shown in Fig. 3.

The simulation of iterative time reversal in one layered heterogeneous media is conducted in this part. Figure 4 depicts a typical realization of the sound velocity of the media, whose mean value is $\mathbb{E}c = 1495\,\mathrm{m/s}$, the standard derivation is about 5%, and the constant density is $\rho = 1000\,\mathrm{kg/m^3}$. The density fluctuation is ignored as it is trivial compared to that of the sound velocity.

In each iteration, the probe pulse is emanated, and the backscattered signal is measured by the transceiver. In order to reduce numerical Gibbs oscillation, a Tukey window is added

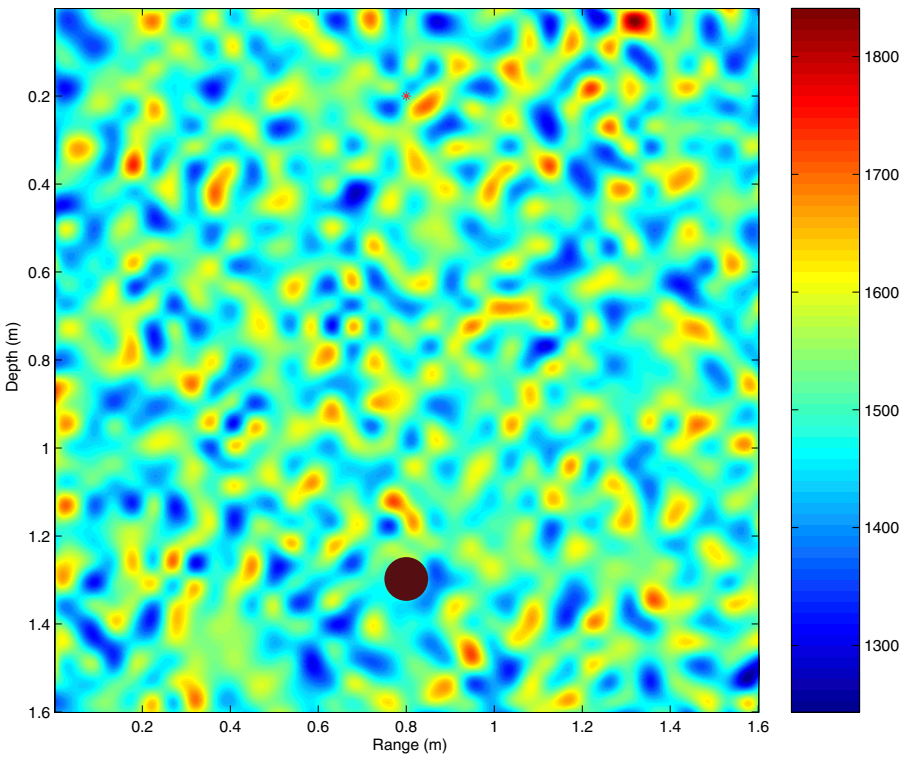

Fig. 4. (Color online) Configuration of the one layered media simulation. A transceiver denoted by the red asterisk is deployed at $(0.8, 0.2)$m, and the liquid sphere with 0.05 m radius is located at $(0.8, 1.3)$m.

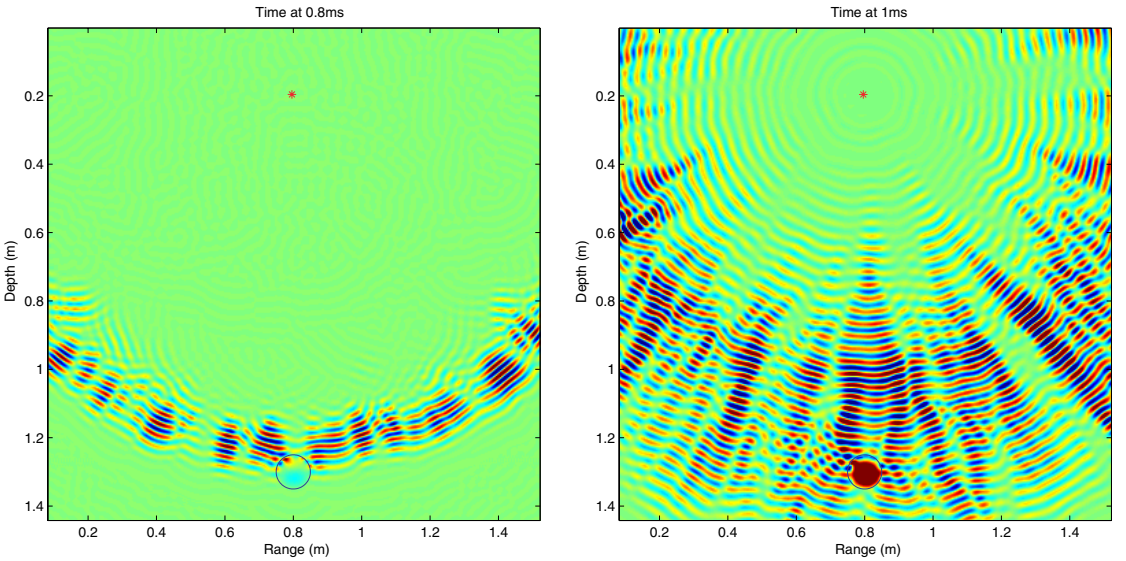

(a) (b)

Fig. 5. (a) A snapshot of the 1st iteration; (b) the 4th iteration in one layered heterogeneous media simulation.

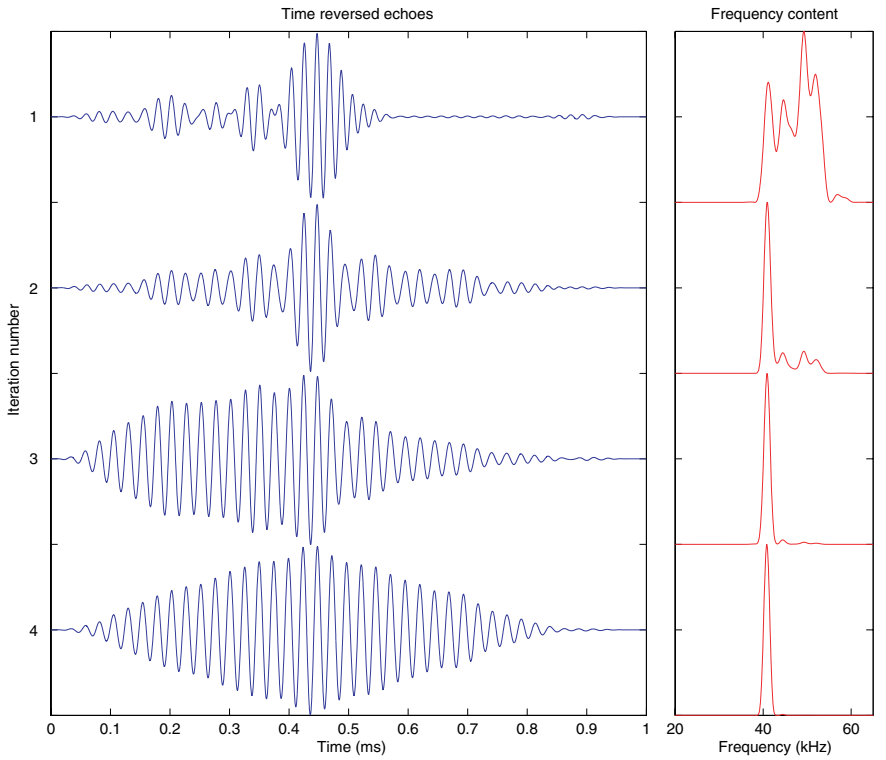

Fig. 6. Time reversed echoes and respective frequency spectra of the first four iterations in one layered heterogeneous media simulation.

to choose the echo waveform, and a $[25, 70]$ kHz Chebyshev type 1 digital bandpass filter is applied to determine the frequency interval.

Figures 5(a) and 5(b) illustrate two snapshots of the 1st and 4th iteration in one layered media simulation, respectively. We can see the wave shape is distorted in heterogeneous media, and the volume clutter will hinder the detection of the target.

Time reversed echoes and respective frequency spectra of the first four iterations are plotted in Fig. 6, and all of them are normalized. We can see the echoes will converge to a resonance mode, whose frequency is at about $f = 40.8$ kHz that corresponds to a peak at $ka = 8.55$ in Fig. 2(b). As spectrum narrowing corresponds to a time-series expanding, the received echoes are prolonged gradually.

3.4. *Two layered media simulation*

In this part, the simulation of iterative time reversal in two layered heterogeneous media is performed. As depicted in Fig. 7, the upper space is replaced by a homogeneous layer, and the normal distributed interface is at the depth of 1.1 m.

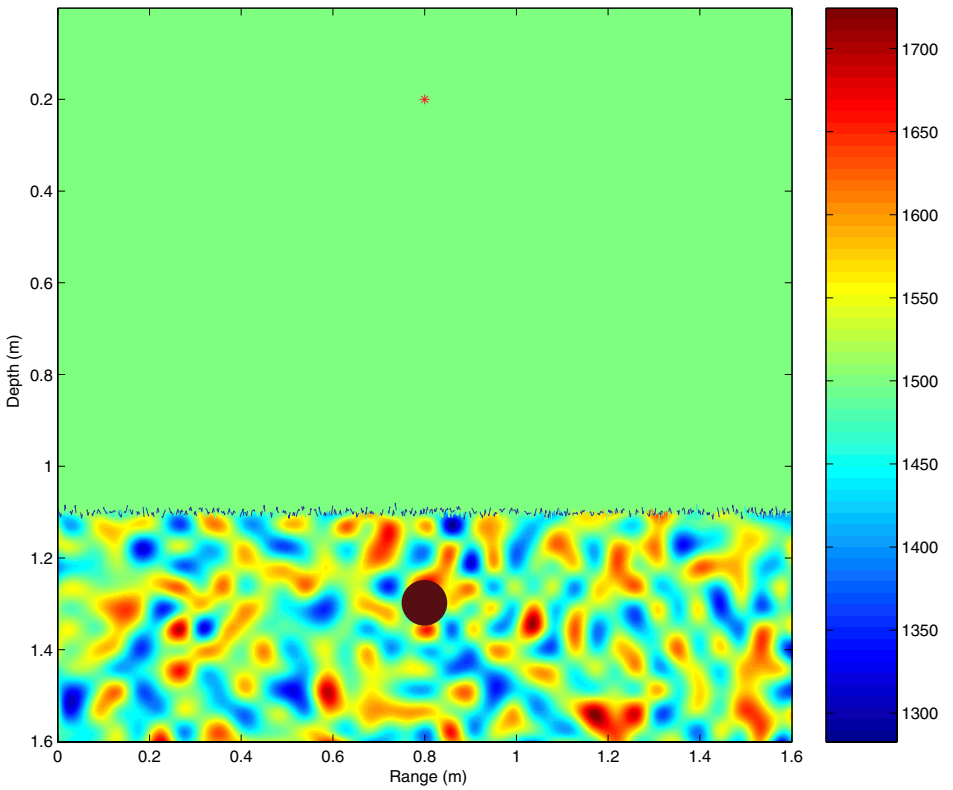

Fig. 7. (Color online) Configuration of the two layered media simulation. A transceiver denoted by the red asterisk is deployed at $(0.8, 0.2)$m, the liquid sphere with 0.05 m radius is located at $(0.8, 1.3)$m, and the interface is at the depth of 1.1 m.

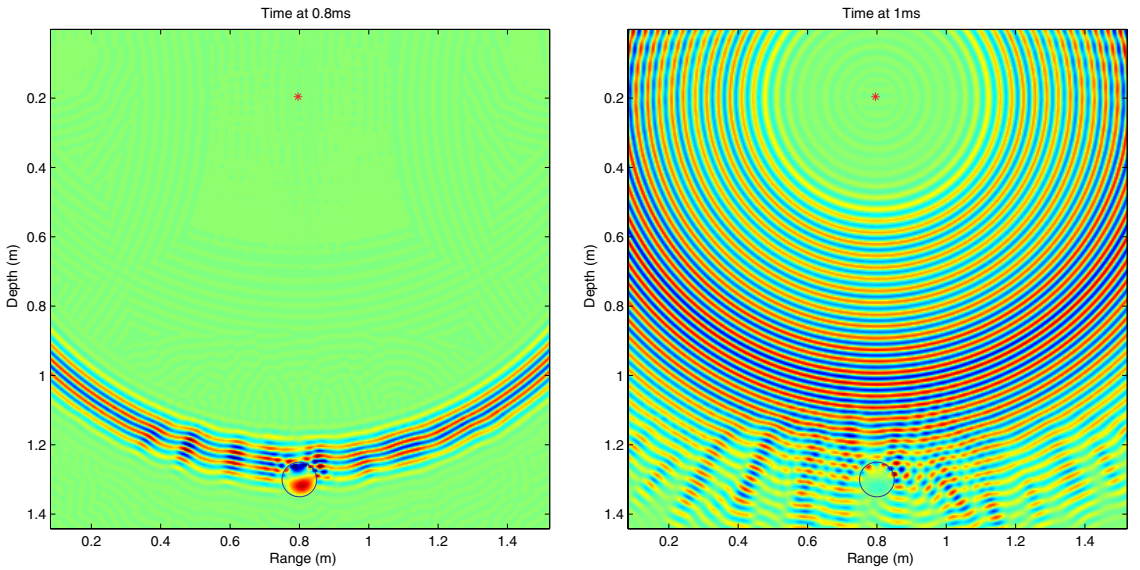

(a) (b)

Fig. 8. (a) A snapshot of the 1st iteration; (b) the 14th iteration in two layered heterogeneous media simulation.

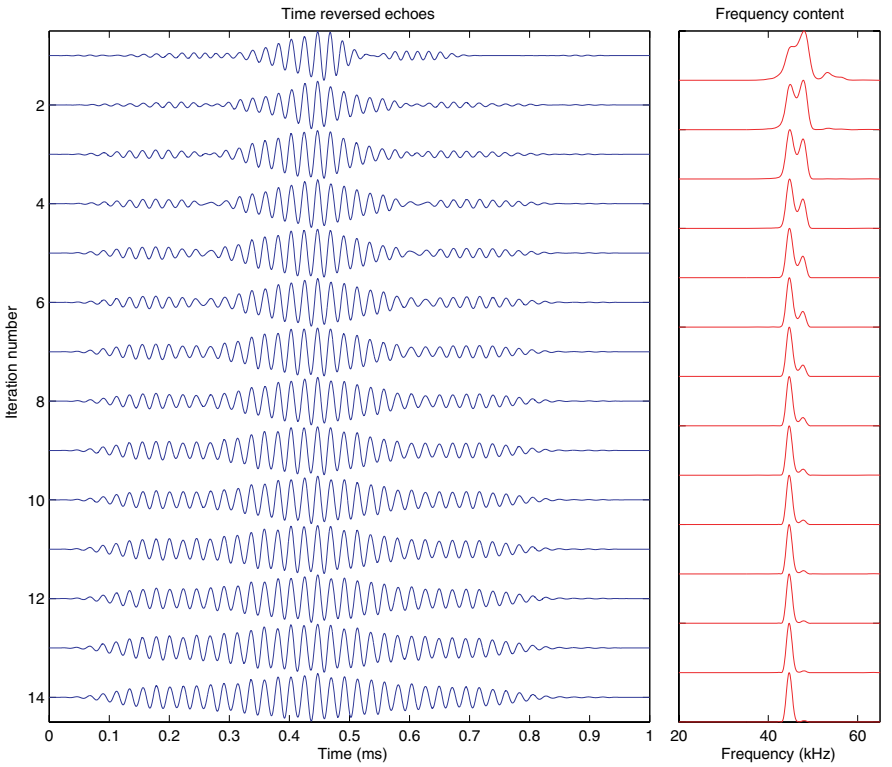

Fig. 9. Time reversed echoes and respective frequency spectra of the first 14 iterations in two layered heterogeneous media simulation.

Figures 8(a) and 8(b) are two snapshots of the 1st and 14th iteration in two layered heterogeneous media simulation, respectively. The rough interface reverberation and volume clutter make it difficult to detect the buried target.

Figure 9 plots the time reversed echoes and respective frequency spectra of the first 14 iterations. We can see as the iteration number increases, the interface response is gradually suppressed, and the echoes will eventually converge to a narrow band signal whose center frequency is at about $f = 44.7\,\text{kHz}$, and the normalized frequency is $ka = 9.36$. The bias is mainly introduced by the multiple scattering effects between the interface and target, and the speed of interface reverberation suppression depends on the ratio of their eigenvalues.

4. Conclusions

The iterative process involving a time reversal mirror is capable of eliminating volume clutter caused by the media fluctuation and suppressing interface reverberation, and will lead echoes to converge to a resonance mode in heterogeneous media. It is fast and can be realized with a single transceiver. The target is detected by exploiting resonance peaks, and the multiple scattering effects will alter the value of converged frequency.

Acknowledgments

The work was supported by the Chinese Academy of Sciences Innovation Foundation CXJJ-260, and the National Natural Science Foundation of China through grant 10604062 and 10874201.

Appendix A. Definition of the Entries of the Reflectivity Coefficient Matrix

According to reciprocity principle, the reflectivity coefficient matrix $\mathbf{c} = \begin{pmatrix} c_{11} & c_{12} & \cdots & c_{1L} \\ c_{21} & c_{22} & \cdots & c_{2L} \\ \vdots & \vdots & \ddots & \vdots \\ c_{L1} & c_{L2} & \cdots & c_{LL} \end{pmatrix}$ is symmetric, and its diagonal entries c_{ll}, for $1 \le l \le L$, are called reflectivity coefficients. For the point-like model at scattering center, the pressure scattered by the lth scatterer $p_l^{\text{sc}}(\omega)\colon \mathbb{R} \to \mathbb{C}$ is equal to the product of the incident pressure $p_l^{\text{in}}(\omega)\colon \mathbb{R} \to \mathbb{C}$ and the reflectivity coefficient $c_{ll}(\omega)\colon \mathbb{R} \to \mathbb{C}$, i.e., $p_l^{\text{sc}}(\omega) = (p_l^{\text{in}} \cdot c_{ll})(\omega)$. That the reflectivity coefficient is a linear map

$$c_{ll}\colon p_l^{\text{in}} \mapsto p_l^{\text{sc}}, \quad l \le L. \tag{A.1}$$

If scatterers are well separated from each other, the reflectivity coefficient matrix $\mathbf{c}$ is diagonal, that the off-diagonal entries are $c_{ll'} = 0$, for all $l \ne l'$. Multiple scattering effects between scatterers are taken into consideration because Green's functions are random in heterogeneous media.

Assume $\mathbf{f} \in \mathbb{C}^L$ is the total pressure incident upon L scatterers, then the scattered pressure is $\tilde{\mathbf{c}}\mathbf{f}$, where $\tilde{\mathbf{c}} = \mathrm{diag}(c_{ll})$. So when the interrogation vector $\mathbf{e} \in \mathbb{C}^M$ is loaded on the array, the backscattered and received pressure is equal to

$$\mathbf{a}_\mathrm{r}\mathbf{g}^\mathrm{t}\tilde{\mathbf{c}}\mathbf{f} = \mathbf{a}_\mathrm{r}\mathbf{g}^\mathrm{t}\mathbf{c}\mathbf{g}\mathbf{a}_\mathrm{e}\mathbf{e}. \tag{A.2}$$

Here we define the direct transfer matrix $\tilde{\mathbf{g}} = \begin{pmatrix} 0 & g_{12} & \cdots & g_{1L} \\ g_{21} & 0 & \cdots & g_{2L} \\ \vdots & \vdots & \ddots & \vdots \\ g_{L1} & g_{L2} & \cdots & 0 \end{pmatrix}$, whose off-diagonals are the Green's functions between scatterers and diagonal entries are flipped to zeros. Then the total pressure incident upon the scatterers is equal to the pressure transferred from the array pluses reflected from others,

$$\mathbf{f} = \mathbf{g}\mathbf{a}_\mathrm{e}\mathbf{e} + \tilde{\mathbf{g}}\tilde{\mathbf{c}}\mathbf{f}. \tag{A.3}$$

Substitute the expression of $\mathbf{g}\mathbf{a}_\mathrm{e}\mathbf{e}$ into Eq. (A.2), and finally we can get the off-diagonal entries of reflectivity coefficient matrix,

$$c_{ll'} = (\mathbf{c})_{ll'} = (\tilde{\mathbf{c}}(\mathbf{i} - \tilde{\mathbf{g}}\tilde{\mathbf{c}})^{-1})_{ll'}, \quad \forall\, l \neq l', \tag{A.4}$$

where the matrix inversion is assumed to be available. If scatterers are well apart, $\mathbf{c} = \tilde{\mathbf{c}}$ is diagonal.

Appendix B. Derivation of the Eigenvalue Expressions of the Time Reversal Matrix

Reflectivity coefficient matrix $\mathbf{c}(\omega)$ can be partitioned as block matrices, i.e., $\mathbf{c} = \begin{pmatrix} \mathbf{c}_{1*} \\ \vdots \\ \mathbf{c}_{l*} \\ \vdots \\ \mathbf{c}_{L*} \end{pmatrix} = (\mathbf{c}_{*1} \cdots \mathbf{c}_{*l} \cdots \mathbf{c}_{*L})$, and the forward and backward diffraction matrix can also be expressed as $\mathbf{g} = \begin{pmatrix} \mathbf{g}_{1*}^\mathrm{t} \\ \vdots \\ \mathbf{g}_{l*}^\mathrm{t} \\ \vdots \\ \mathbf{g}_{L*}^\mathrm{t} \end{pmatrix}$ and $\mathbf{g}^\mathrm{t} = (\mathbf{g}_{1*} \cdots \mathbf{g}_{l*} \cdots \mathbf{g}_{L*})$, respectively. Then we can get the lth eigenvalue from Eq. (10),

$$\begin{aligned} \lambda_l &= \bar{\mathbf{g}}_{l*}^\mathrm{t}\mathbf{h}^*\mathbf{h}\bar{\mathbf{g}}_{l*} \\ &= \bar{\mathbf{g}}_{l*}^\mathrm{t} \left(\mathbf{a}_\mathrm{r}(\mathbf{g}_{1*} \cdots \mathbf{g}_{l*} \cdots \mathbf{g}_{L*})\mathbf{c} \begin{pmatrix} \mathbf{g}_{1*}^\mathrm{t} \\ \vdots \\ \mathbf{g}_{l*}^\mathrm{t} \\ \vdots \\ \mathbf{g}_{L*}^\mathrm{t} \end{pmatrix} \mathbf{a}_\mathrm{e} \right)^* \left(\mathbf{a}_\mathrm{r}(\mathbf{g}_{1*} \cdots \mathbf{g}_{l*} \cdots \mathbf{g}_{L*})\mathbf{c} \begin{pmatrix} \mathbf{g}_{1*}^\mathrm{t} \\ \vdots \\ \mathbf{g}_{l*}^\mathrm{t} \\ \vdots \\ \mathbf{g}_{L*}^\mathrm{t} \end{pmatrix} \mathbf{a}_\mathrm{e} \right) \bar{\mathbf{g}}_{l*}^* \end{aligned}$$

$$
\begin{aligned}
&= |a_{\mathrm{e}}a_{\mathrm{r}}|^2 \left(0 \cdots \|\mathbf{g}_{l*}\| \cdots 0\right) \mathbf{c}^* \begin{pmatrix} \|\mathbf{g}_{1*}\|^2 & & \\ & \ddots & \\ & & \|\mathbf{g}_{L*}\|^2 \end{pmatrix} \mathbf{c} \begin{pmatrix} 0 \\ \vdots \\ \|\mathbf{g}_{l*}\| \\ \vdots \\ 0 \end{pmatrix} \\
&= |a_{\mathrm{e}}a_{\mathrm{r}}|^2 \|\mathbf{g}_{l*}\|^2 \mathbf{c}_{l*}^* \begin{pmatrix} \|\mathbf{g}_{1*}\|^2 & & \\ & \ddots & \\ & & \|\mathbf{g}_{L*}\|^2 \end{pmatrix} \mathbf{c}_{*l} \\
&= |a_{\mathrm{e}}a_{\mathrm{r}}|^2 \|\mathbf{g}_{l*}\|^2 \sum_{l'=1}^{L} \|\mathbf{g}_{l'*}\|^2 c_{ll'}^* c_{l'l} \\
&= |a_{\mathrm{e}}a_{\mathrm{r}}|^2 \|\mathbf{g}_{l*}\|^2 \sum_{l'=1}^{L} \|\mathbf{g}_{l'*}\|^2 |c_{ll'}|^2, \quad l \le L.
\end{aligned} \tag{B.1}
$$

Here we get it.

References

1. Peter Blomgren, George Papanicolaou and Hongkai Zhao, Super-resolution in time-reversal acoustics, *J. Acoust. Soc. Am.* **111**(1) (2002) 230–248.
2. Chrysoula Tsogka and George C. Papanicolaou, Time reversal through a solid-liquid interface and super-resolution, *Inverse Problems* **18**(6) (2002) 1639–1657.
3. Liliana Borcea, George Papanicolaou, Chrysoula Tsogka and James Berryman, Imaging and time reversal in random media, *Inverse Problems* **18**(5) (2002) 1247–1279.
4. Mathias Fink and Julien de Rosny, Time-reversed acoustics in random media and in chaotic cavities, *Nonlinearity* **15**(1) (2002) R1–R18.
5. José M. F. Moura, Yuanwei Jin, Daniel Stancil, Jian-Gang Zhu, Ahmet Cepni, Yi Jiang and Benjamin Henty, Single antenna time reversal adaptive interference cancellation, in *Proc. International Conference on Acoustics, IEEE* Vol. 4 (2005) 1121–1124.
6. L. Flax, L. R. Dragonette and H. Uberall, Theory of elastic resonance excitation by sound scattering, *J. Acoust. Soc. Am.* **63**(3) (1978) 723–731.
7. K. Jerome Diercks and R. Hickling, Echoes from hollow aluminum spheres in water, *J. Acoust. Soc. Am.* **41**(2) (1967) 380–393.
8. M. Maleki, Acoustic resonance scattering from a submerged anisotropic sphere, *Acoust. Phys.* **54**(2) (2008) 168–179.
9. C. Prada, F. Wu and M. Fink, The iterative time reversal mirror: A solution to self-focusing in the pulse echo mode, *J. Acoust. Soc. Am.* **90**(2) (1991) 1119–1129.
10. Claire Prada, Jean-Louis Thomas and Mathias Fink, The iterative time reversal process: Analysis of the convergence, *J. Acoust. Soc. Am.* **97**(1) (1995) 62–71.
11. David Isaacson, Margaret Cheney and Matti Lassas, Optimal acoustic measurements, *SIAM J. Appl. Math.* **61**(5) (2001) 1628–1647.

12. L. Pautet, A. Tesei, P. Guerrini and E. Pouliquen, Target echo enhancement using a single-element time reversal mirror, *IEEE J. Oceanic. Eng.* **30**(4) (2005) 912–920.
13. D. M. Pierson, Buried-object detection using time-reversed acoustics, PhD thesis, North Carolina State University (2003).
14. N. D. Veksler, *Resonance Acoustic Spectroscopy* (Springer-Verlag, New York, 1993).